Supporting Information

Boosting Light-driven Pyroelectric Response of Poly(vinylidene difluoride) by constructing Mn-doped BZT-BCT/PVDF Composites

Lu Wang[a], Feilong Yan[c], Jifeng Pan[a], Xiang He[a], Chen Chen[a], Muzaffar Ahmad Boda[a], Zhiguo Yi[a,b]*

[a]State Key Laboratory of High Performance Ceramics and Superfine Microstructure, Shanghai Institute of Ceramics, Chinese Academy of Sciences, Shanghai 200050, China

[b]Center of Materials Science and Optoelectronics Engineering, University of Chinese Academy of Sciences, Beijing 100049, China

[c]Key Laboratory of Optoelectronic Material and Device, Department of Physics, Shanghai Normal University, Shanghai 200234, China

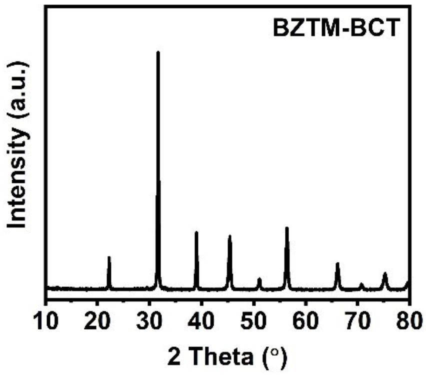

Fig. S1. The XRD pattern of BZTM-BCT particles.

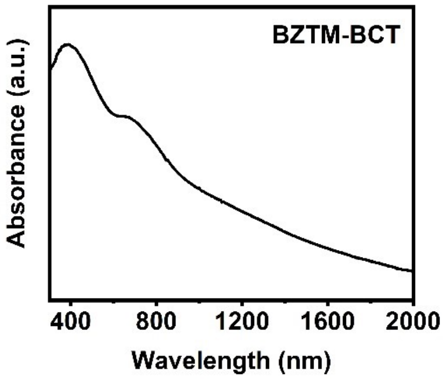

Fig. S2. The UV-Visible absorbance spectrum of the BZTM-BCT particles.

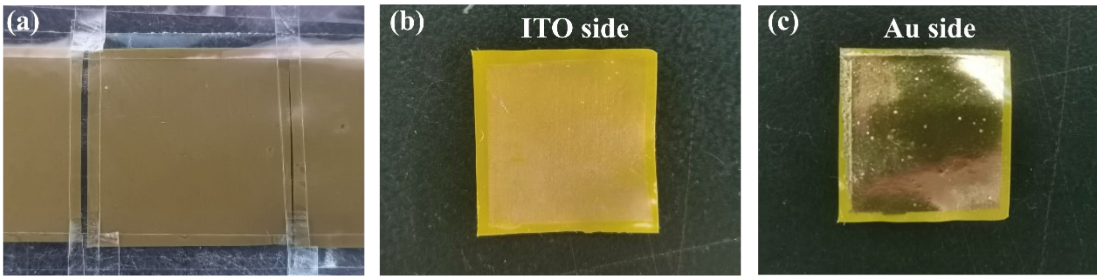

Fig. S3. Electrode deposition. (a) The fixed films with tape before depositing electrodes. (b) ITO electrode side. (c) Au electrode side

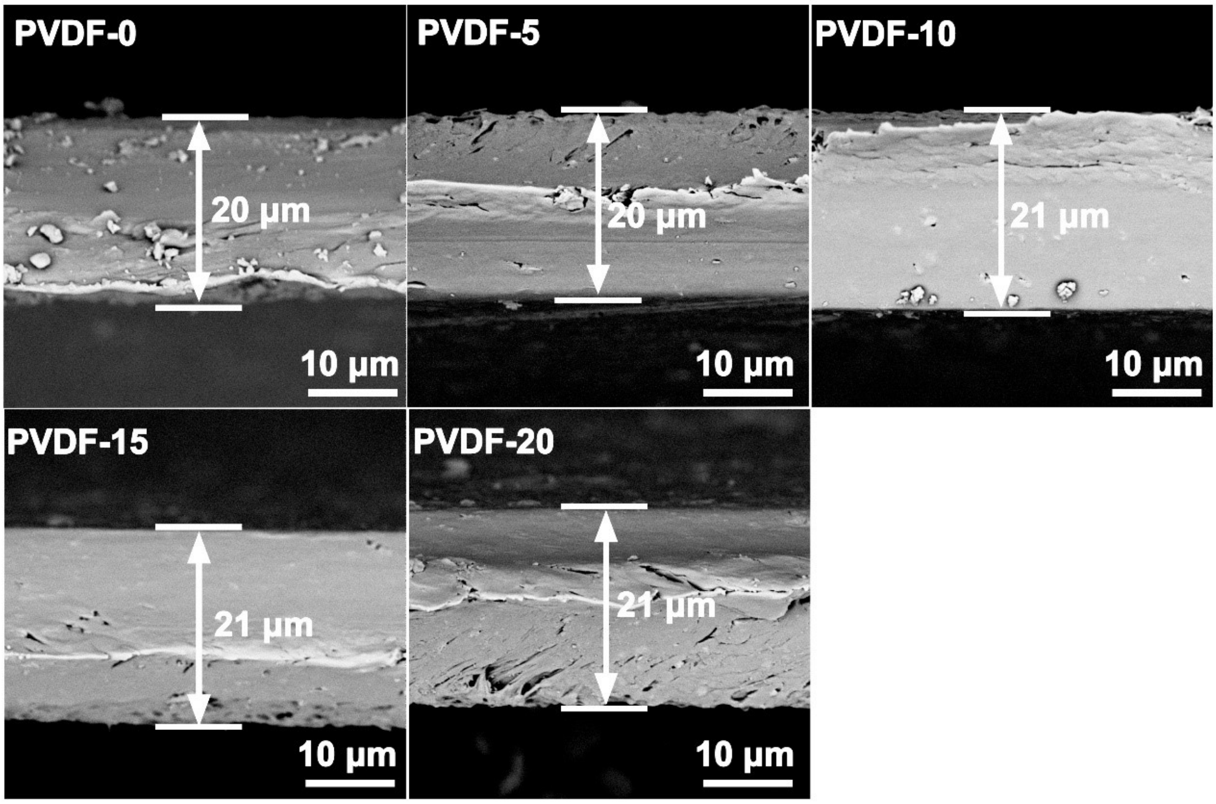

Fig. S4. The cross-section morphology of the PVDF-*x* films.

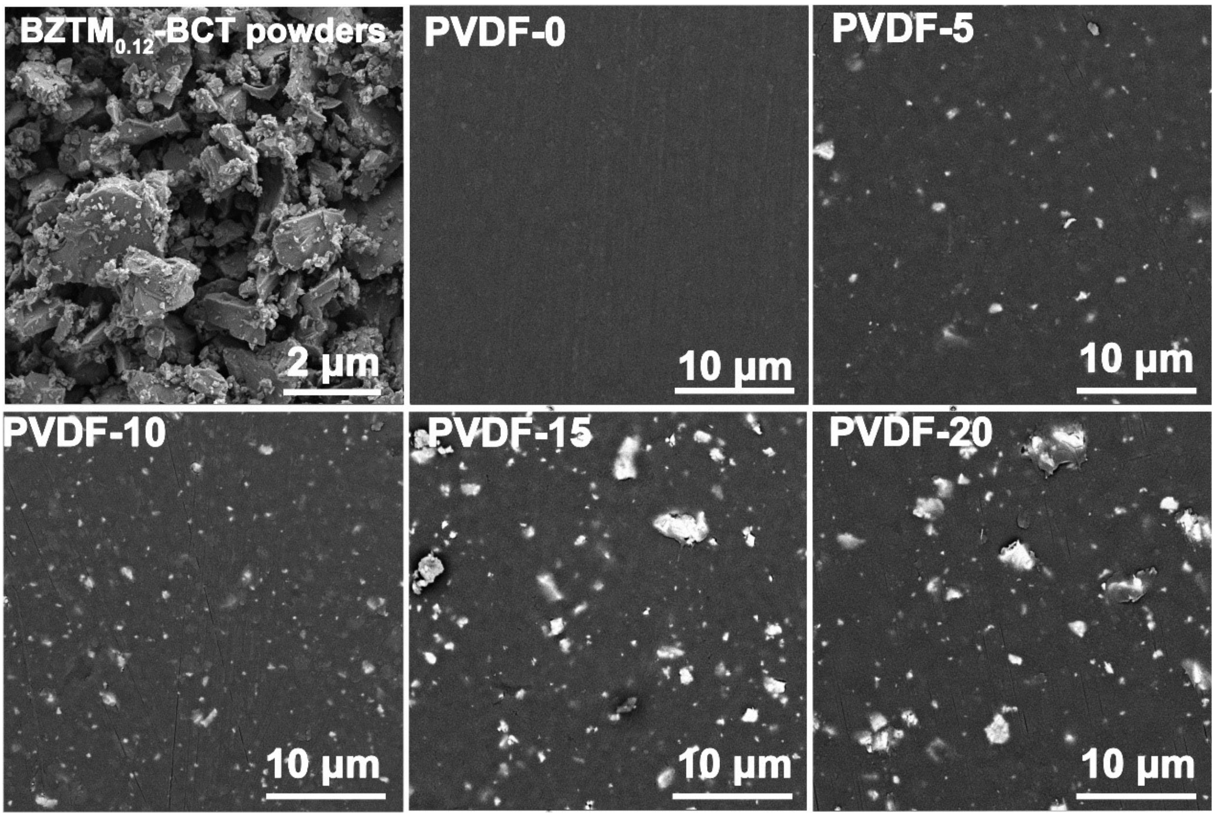

Fig. S5. Surface morphological characterization. (a) The granule morphology of the $BZTM_{0.12}$-BCT powders. (b-f) Microscopic morphology of PVDF-*x* composite films with different $BZTM_{0.12}$-BCT content: *x* = 0 (b); *x* = 5 (c); *x* = 10 (d); *x* = 15 (e); *x* = 20 (f).

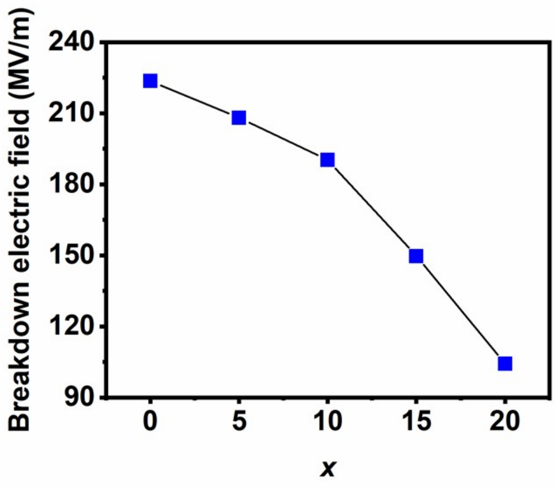

Fig. S6. Breakdown electric fields of PVDF-*x* films.

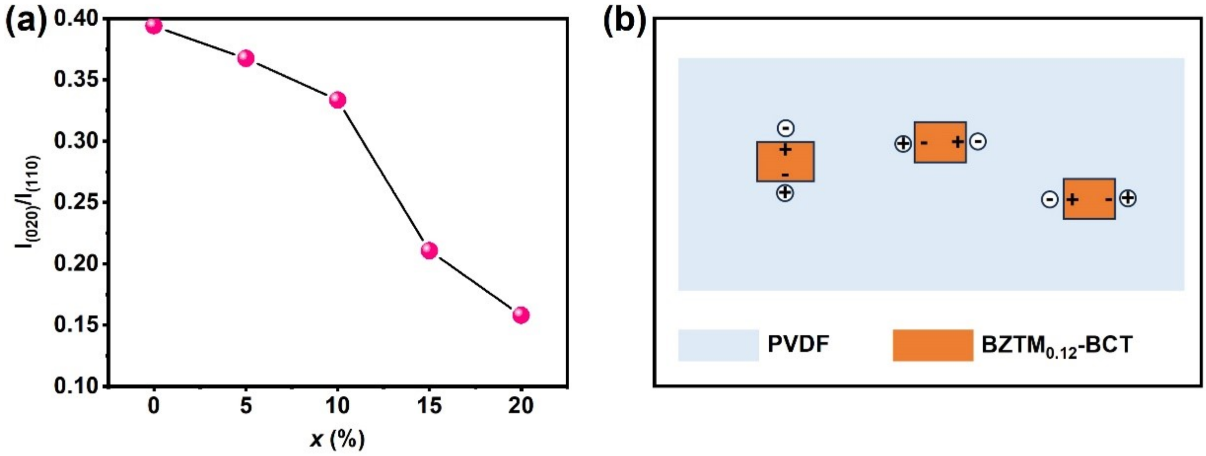

Fig. S7. Phase structure change of PVDF-*x* films with *x*. (a) the ratio of diffraction peak intensities between (020) and (110) planes, indicating that the content of β phase gradually increases with increasing the $BZTM_{0.12}$-BCT ceramic particles. (b) Schematic diagram illustrating that the ferroelectric ceramic powders induce the polar phase in the PVDF-*x* films.

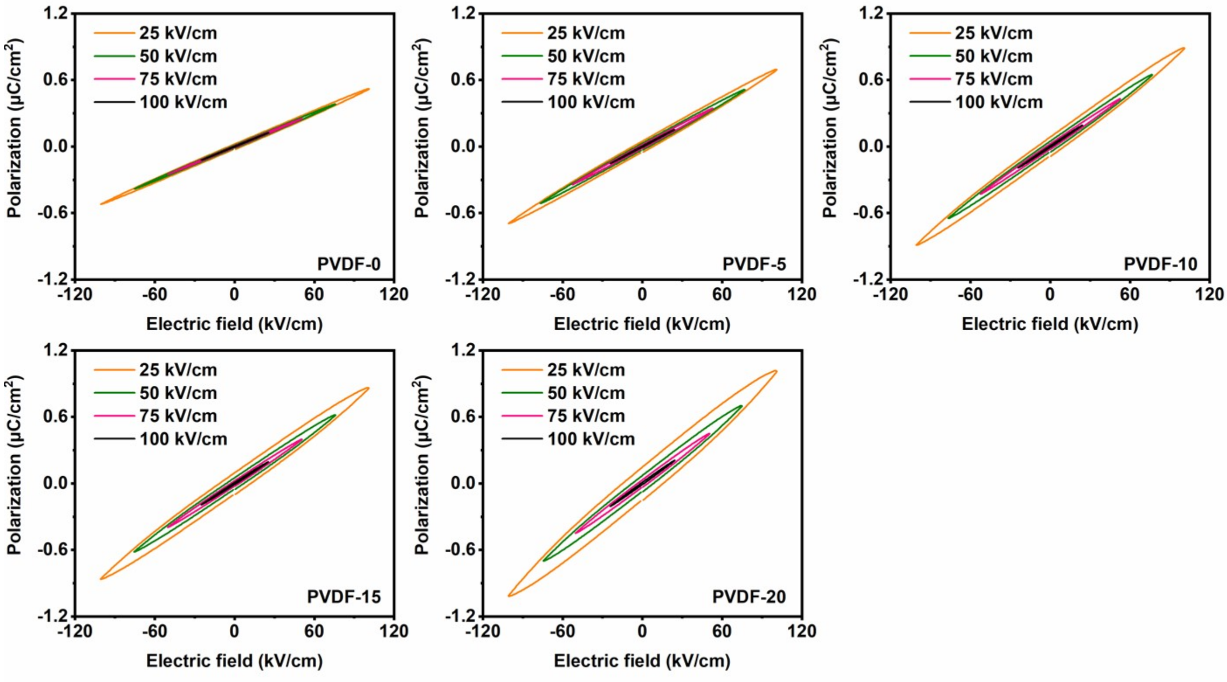

Fig. S8. Ferroelectric properties of PVDF-*x* films under different electric fields.

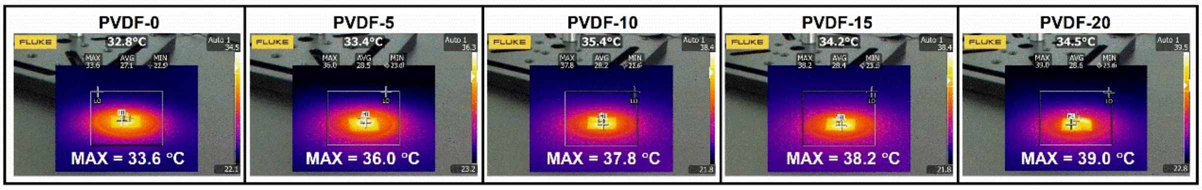

Fig. S9. The temperature of the PVDF-*x* films after 365 nm LED light illuminating for 30 s, tested by an infrared thermal image instrument.

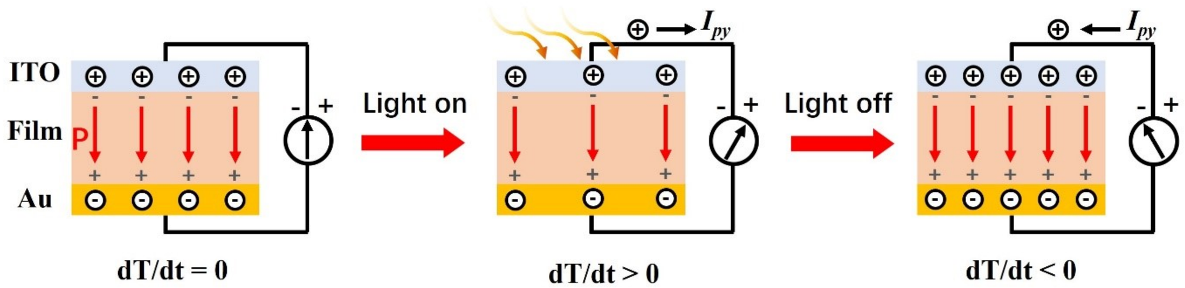

Fig. S10. Photo-pyroelectric response mechanism of the PVDF composite film.

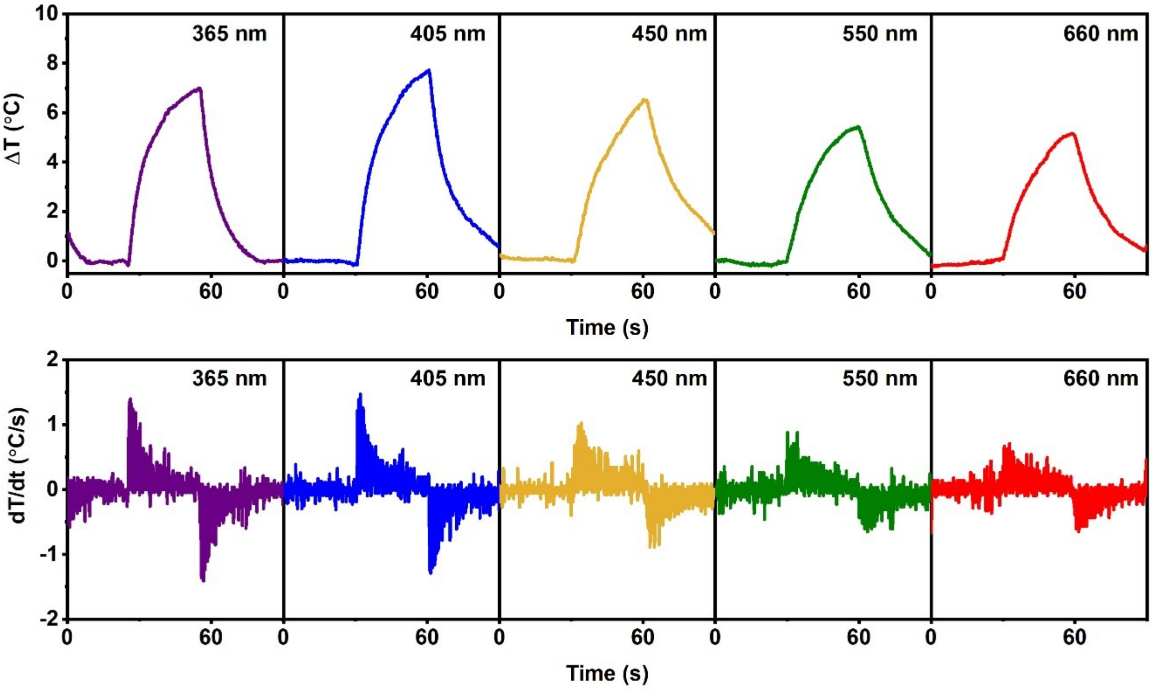

Fig. S11. The photo wavelength dependent photo indeuced temperature change of PVDF-10 film.

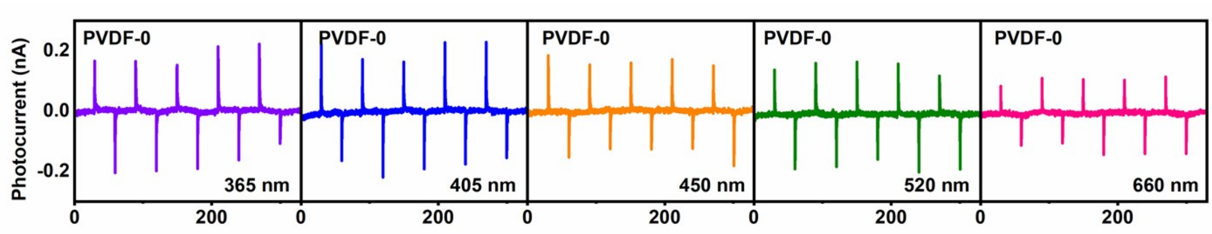

Fig. S12. The photo wavelength dependent photo-pyroelectric current of the pure PVDF film. The light intensity for all the used lights is fixed at 100 mW/cm^2.

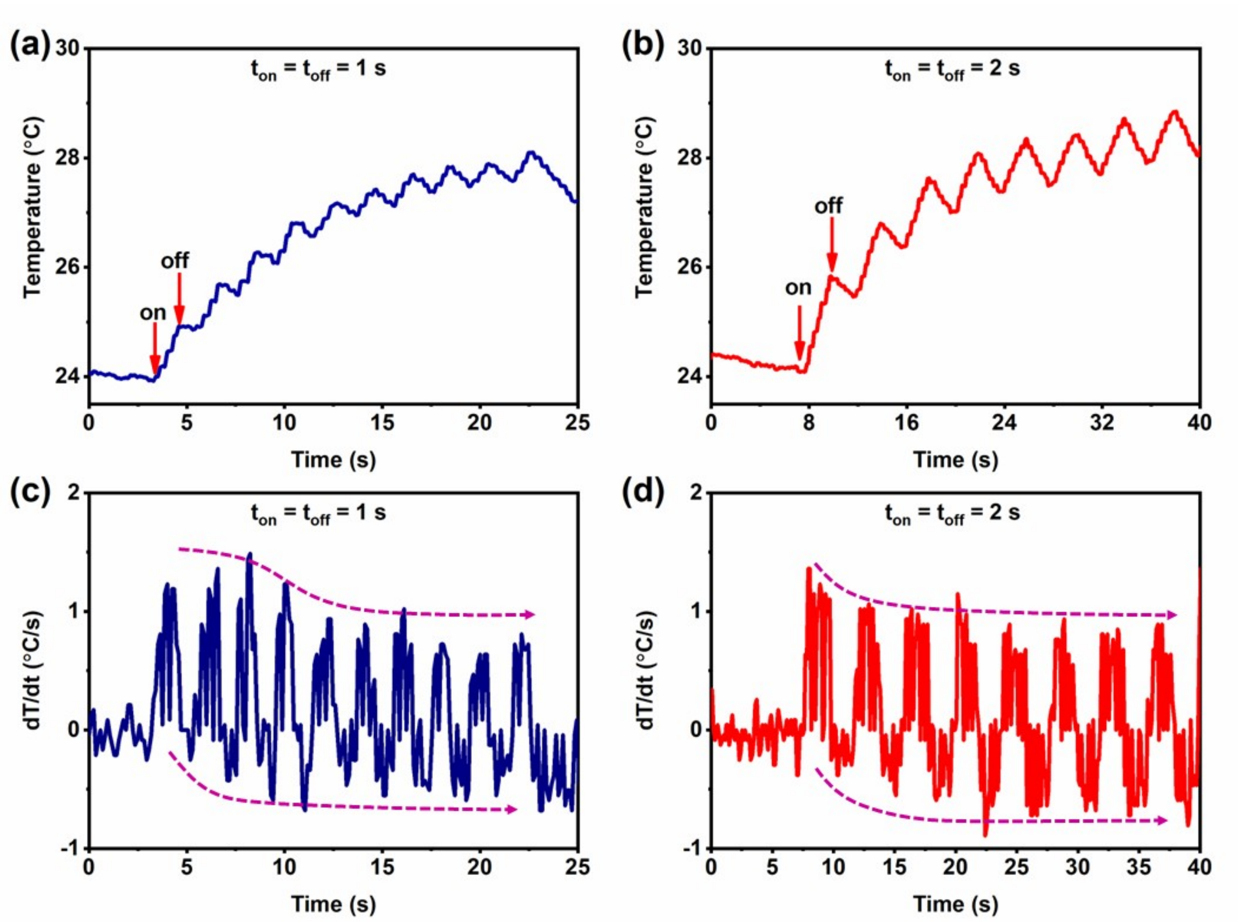

Fig. S13. The temperature response with changing the t_{on} and t_{off} ($t_{on} = t_{off}$) under 365 nm LED light with light intensity of 100 mW/cm^2. (a,b) temperature variation (c,d) and temperature change rate when $t_{on} = t_{off} = 1$ s (a,c) and $t_{on} = t_{off} = 2$ s (b,d).

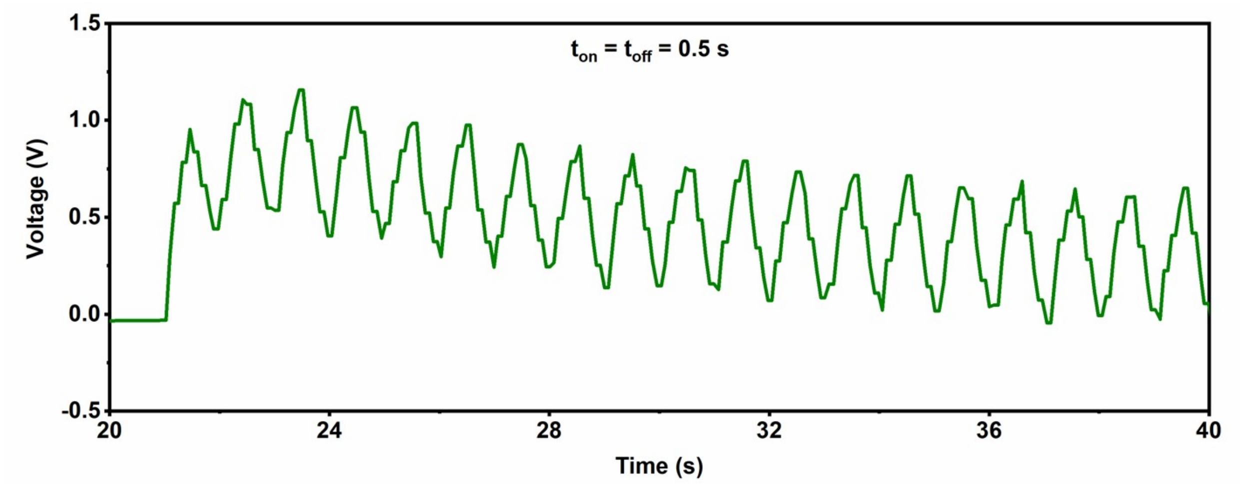

Fig. S14. The voltage evolution as the light illumination continued in situation (i).

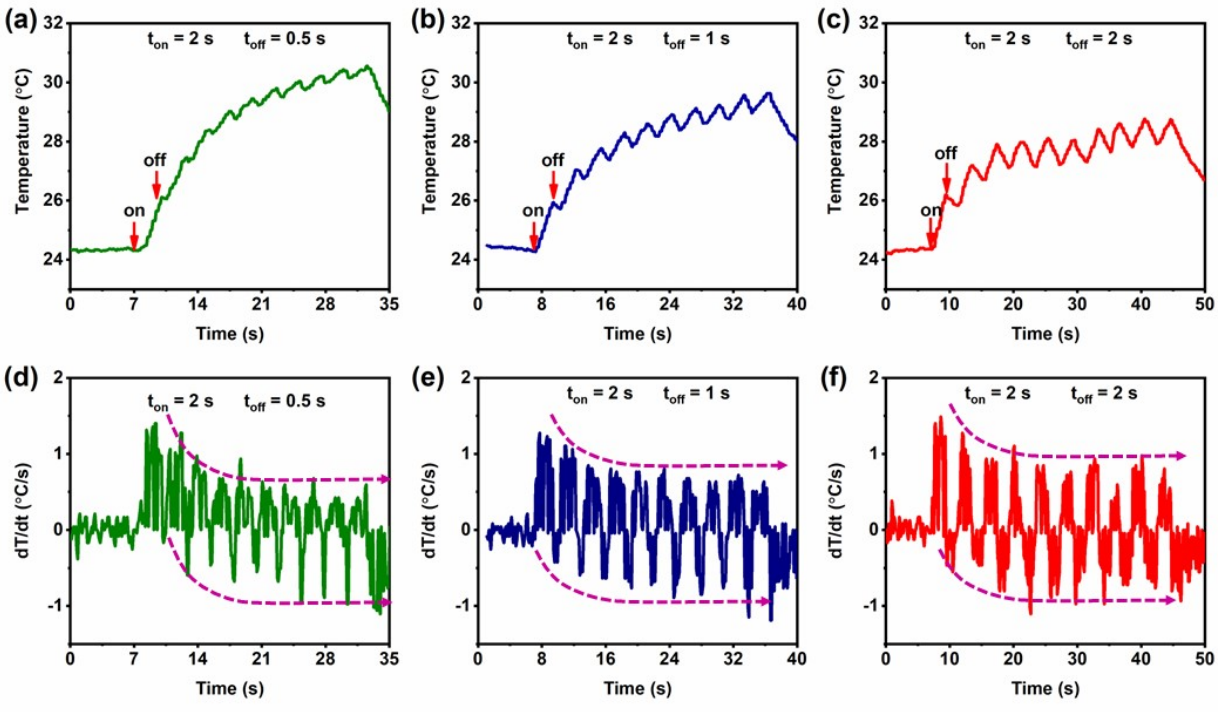

Fig. S15. The temperature response with changing the t_{on} and t_{off} (fixing t_{on}, changing t_{off}) under 365 nm LED light with light intensity of 100 mW/cm^2. (a-c) temperature variation and (d-f) temperature change rate when t_{on} = 2 s, t_{off} = 0.5 s (a,d), 1.0 s (b,e), 2.0 s (c,f).

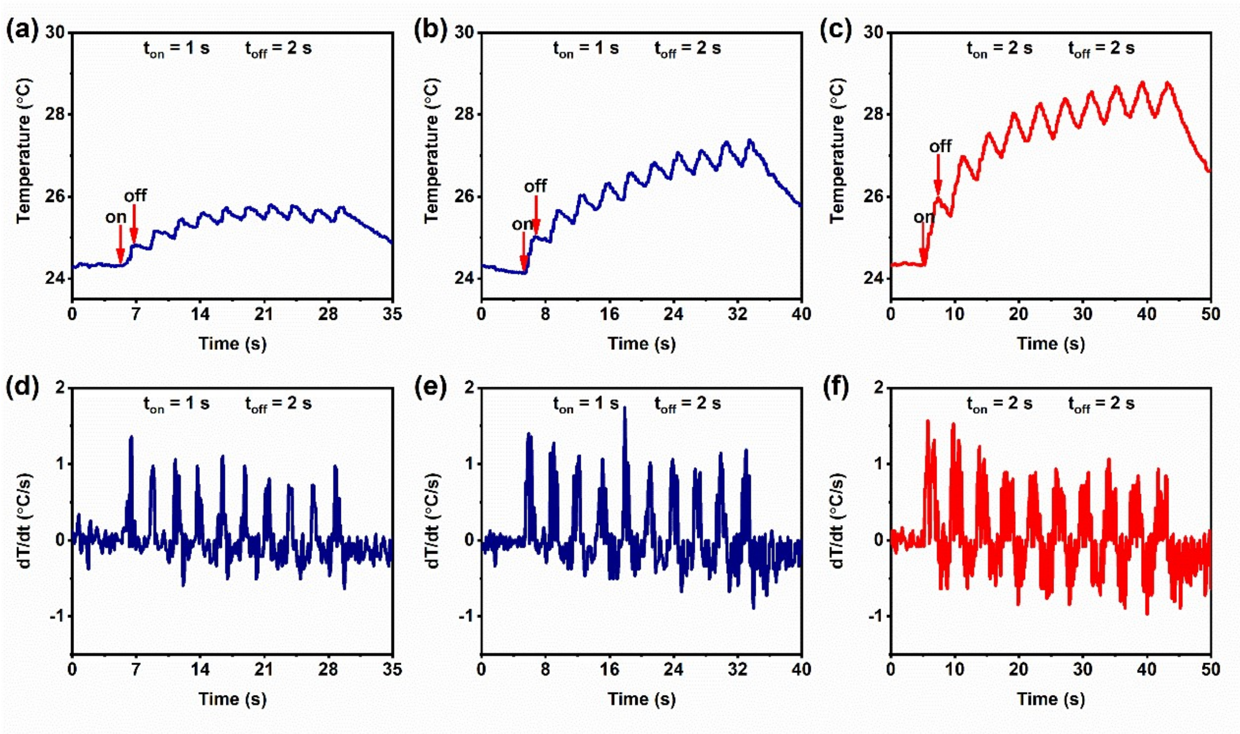

Fig. S16. The temperature response with changing the t_{on} and t_{off} (fixing t_{off}, changing t_{on}) under 365 nm LED light with light intensity of 100 mW/cm^2. (a-c) temperature variation and (d-f) temperature change rate when t_{off} = 2 s, t_{on} = 0.5 s (a,d), 1.0 s (b,e), 2.0 s (c,f).

Table S1 The content of β phase and crystallinity of PVDF-*x* films

Sample	Content of β phase			Crystallinity		
	A_{α}	$A_{\beta+\gamma}$	F_{EA}	ΔH_m (J/g)	φ	X_c
PVDF-0	0.54	3.02	81.6%	52.83	0	50.51%
PVDF-5	0.31	2.96	88.3%	55.85	0.05	56.04%
PVDF-10	0.21	2.90	91.6%	55.93	0.10	59.41%
PVDF-15	0.18	2.76	92.4%	50.99	0.15	57.35%
PVDF-20	0.15	2.73	92.8%	45.10	0.20	53.78%

Table S2 Optical responsiveness and detectivity of PVDF-10 film.

	Light wavelength				
	365 nm	405 nm	450 nm	520 nm	660 nm
Responsiveness (mA/W)	2.7×10^{-5}	2.7×10^{-5}	2.2×10^{-5}	1.8×10^{-5}	1.6×10^{-5}
Detectivity (Jones)	2.3×10^{6}	2.3×10^{6}	1.9×10^{6}	1.5×10^{6}	1.4×10^{6}

Table S3 Comparison of PVDF based photodetectors.

Compositions	Light wavelength	Light intensity mW cm^{-2}	Output current nA/cm^2	Reference
Graphene/PVDF/Al	808 nm	2000	6.25	[1]
CNT/PVDF/Al	808 nm	1450	7	[2]
Patterned Al/PVDF/Al	NIR	~1000	6.6	[3]
Graphene/PVDF/Al	IR	340	10	[4]
Au@rGO-PEI/Ag/pvdf/Ag	Sunlight	100	25.8	[5]
PEDOT:Tos/PVDF/PEDOT:Tos	NIR	60	1.93	[6]
Graphene/$Cs_{0.33}WO_3$/Ag/PVDF/Ni-Cu	IR	226	7.4	[7]
Ni/PVDF/$MAPbI_3$/Cu	IR	~1000	0.004	[8]
ITO/PVDF-TrFE/KNN/Ag	405 nm	56	3.765	[9]
ITO/PVDF/BZTM-BCT/Au	365 nm	100	2.67	This work

Reference

[1] H. Liu, T. Zhao, W. Jiang, R. Jia, D. Niu, G. Qiu, L. Fan, X. Li, W. Liu, B. Chen, Y. Shi, L. Yin, B. Lu, Flexible Battery-Less Bioelectronic Implants: Wireless Powering and Manipulation by Near-Infrared Light., Adv. Funct. Mater. 25 (2015) 7071-7079. https://doi.org/10.1002/adfm.201502752.

[2] T. Zhao, W. Jiang, H. Liu, D. Niu, X. Li, W. Liu, X. Li, B. Chen, Y. Shi, L. Yin, B. Lu, An infrared-driven flexible pyroelectric generator for non-contact energy harvester, Nanoscale 8 (2016) 8111-8117. https://doi.org/10.1039/C5NR09290F.

[3] D. Zabek, J. Taylor, E. L. Boulbar, C. R. Bowen, Micropatterning of Flexible and Free Standing Polyvinylidene Difluoride (PVDF) Films for Enhanced Pyroelectric Energy Transformation, Adv. Energy Mater. 5 (2015) 1401891. https://doi.org/10.1002/aenm.201401891

[4] D. Zabek, K. Seunarine, C. Spacie, C. Bowen, Graphene Ink Laminate Structures on Poly(vinylidene difluoride) (PVDF) for Pyroelectric Thermal Energy Harvesting and Waste Heat Recovery, ACS Appl. Mater. Interfaces 9 (2017) 9161-9167. https://doi.org/10.1021/acsami.6b16477

[5] H. Li, H. Wang, X. Li, J. Huang, X. Li, S. K. Boong, H. K. Lee, J. Han, R. Guo, Boosting solar-to-pyroelectric energy harvesting via a plasmon-enhanced solar-thermal conversion approach. Nano Energy 100 (2022) 107527. https://doi.org/10.1016/j.nanoen.2022.107527.

[6] J. Lee, H. J. Kim, Y. J. Ko, J. Y. Baek, G. Shin, J. G. Jeon, J. H. Lee, J. H. Kim, J. H. Jung,

T. J. Kang, Enhanced pyroelectric conversion of thermal radiation energy: Energy harvesting and non-contact proximity sensor. Nano Energy 97 (2022) 107178. https://doi.org/10.1016/j.nanoen.2022.107178

[7] M. R. Gokana, C.-M. Wu, K. G. Motora, J. Y. Qi, W.-T. Yen. Effects of patterned electrode on near infrared light-triggered cesium tungsten bronze/poly(vinylidene)fluoride nanocomposite-based pyroelectric nanogenerator for energy harvesting, J. Power Sources 536 (2022)231524. https://doi.org/10.1016/j.jpowsour.2022.231524

[8] A. Sultana, S. K. Ghosh, M. M. Alam, P. Sadhukhan, K. Roy, M. Xie, C. R. Bowen, S. Sarkar, S. Das, T. R. Middya, D. Mandal. Methylammonium Lead Iodide Incorporated Poly(vinylidene fluoride) Nanofibers for Flexible Piezoelectric-Pyroelectric Nanogenerator. ACS Appl Mater Interfaces 11 (2019) 27279-27287. https://doi.org/10.1021/acsami.9b04812

[9] C. Wang, Y. Zhang, B. Zhang, B. Wang, J. Zhang, L. Q. Chen, Q. Zhang, Z. L. Wang, K. Ren, Flexophotovoltaic Effect in Potassium Sodium Niobate/Poly(Vinylidene Fluoride-Trifluoroethylene), Nanocomposite. Adv. Sci. 8 (2021) 2004554. https://doi.org/10.1002/advs.202004554